Title
Characterization of Metabolic Differences between Benign and Malignant Tumors: High-Spectral-Resolution Diffuse Optical Spectroscopy

Journal
Radiology, 254(1)

ISSN
0033-8419

Authors
Kukreti, Shwayta
Cerussi, Albert E
Tanamai, Wendy
et al.

Publication Date
2010

DOI
10.1148/radiol.09082134

Characterization of Metabolic Differences between Benign and Malignant Tumors: High-Spectral-Resolution Diffuse Optical Spectroscopy[1]

Shwayta Kukreti, PhD
Albert E. Cerussi, PhD
Wendy Tanamai, BS
David Hsiang, MD
Bruce J. Tromberg, PhD
Enrico Gratton, PhD

Purpose: To develop a near-infrared spectroscopic method to identify breast cancer biomarkers and to retrospectively determine if benign and malignant breast lesions could be distinguished by using this method.

Materials and Methods: The study was HIPAA compliant and was approved by the university institutional review board. Written informed consent was obtained. By using self-referencing differential spectroscopy (SRDS) analysis, the existence of specific spectroscopic signatures of breast lesions on images acquired by using diffuse optical spectroscopy imaging in the wavelength range (650–1000 nm) was established. The SRDS method was tested in 60 subjects (mean age, 38 years; age range, 22–74 years). There were 17 patients with benign breast tumors and 22 patients with malignant breast tumors. There were 21 control subjects.

Results: Discrimination analysis helped separate malignant from benign tumors. A total of 40 lesions (22 malignant and 18 benign) were analyzed. Twenty were true-positive lesions, 17 were true-negative lesions, one was a false-positive lesion, and two were false-negative lesions (sensitivity, 91% [20 of 22]; specificity, 94% [17 of 18]; positive predictive value, 95% [20 of 21]; and negative predictive value, 89% [17 of 19]).

Conclusion: The SRDS method revealed localized tumor biomarkers specific to pathologic state.

Supplemental material: *http://radiology.rsna.org/lookup/suppl/doi:10.1148/radiol.2541082134/-/DC1*

[1] From the Beckman Laser Institute, University of California, Irvine, Calif (S.K., A.E.C., W.T., B.J.T., E.G.); Laboratory for Fluorescence Dynamics, University of California, Irvine, 3210 Natural Sciences II Building, Irvine CA 92612 (S.K., E.G.); College of Medicine at the University of Illinois, Urbana-Champaign, Ill (S.K.); Biophysics and Computational Biology Program, University of Illinois, Urbana-Champaign, Ill (S.K., E.G.); Department of Biomedical Engineering, University of California, Irvine, Calif (B.J.T., E.G.); Laser Medical and Microbeam Program, University of California, Irvine, Calif (A.E.C., B.J.T.); and Department of Oncological Surgery, University of California, Irvine Medical Center, Orange, Calif (D.S.). Received December 10, 2008; revision requested February 4, 2009; revision received April 27; accepted July 1; final version accepted July 20. Supported by the Laser Microbeam and Medical Program (P41-RR01192), California Breast Cancer Research Program, and Chao Family Comprehensive Cancer Center (P30-CA62203). **Address correspondence to** E.G. (e-mail: *egratton22@yahoo.com*).

Spectroscopic results add functional and molecular-specific information to imaging. For example, several in vivo magnetic resonance (MR) spectroscopy studies (1–9) have shown that tumors exhibit peaks at 3.2 ppm in hydrogen 1 spectra of breast tissue that correspond to elevated levels of total choline which are known to be more abundant in active tumors. MR spectroscopy may improve diagnostic accuracy in the distinction between malignant and benign tumors and help predict therapeutic response in treated tumors (10–12).

Diffuse optical imaging is commonly used to provide biochemical information on hemoglobin concentration by measuring near-infrared (NIR) tissue absorption (13–18). Studies have shown diffuse optical imaging used to depict breast tumors and monitor tumor response to therapy (19,20). Diffuse optical spectroscopy (DOS) imaging, by increasing the wavelength range and resolution, helps measure not only the abundance of hemoglobin but also bulk lipids and water (21). DOS imaging has been used to characterize malignant tumors and tumor response to chemotherapy (22–24). However, tumor characterization by using these components (hemoglobin, water, and bulk lipids) has not been found to be specific for malignancy: The abundance of these tissue chromophores is not a unique cancer-specific signature (16,21,25). Furthermore, age and hormonal status introduce high interpatient variability in NIR absorption spectra and complicate diagnosis when only the magnitude of tissue absorption is used (24,26,27).

Through the application of a spectral analysis method that accounts for interpatient variability, we have discovered metabolic differences between malignant and normal tissues that result from subtle changes in molecular disposition (28). Our purpose was to demonstrate how absorption signatures, likely resulting from changes in lipid, hemoglobin, and water metabolism, rather than the abundance of molecules, help distinguish between benign and malignant breast tumors.

Advances in Knowledge

- A self-referencing differential spectroscopy (SRDS) method has been developed for near-infrared (NIR) (650–1000 nm) diffuse optical spectroscopic (DOS) imaging in tissues that accounts for the unique metabolism of individual patients and facilitates comparisons across patient populations.
- The SRDS method exploits the presence or absence of a spectral fingerprint that reports on molecular disposition—the location, concentration, and environment of a molecular species—and not molecular abundance of NIR absorbers in tissues (hemoglobin, water, and lipids).
- DOS imaging measurements of breast lesions display unique endogenous spectral absorption fingerprints, called specific tumor components (STCs), that separate lesions from normal breast tissues.
- A weighted wavelength analysis method was developed to exploit the entire STC absorption spectrum in the NIR to discriminate between benign and malignant tumors.

Materials and Methods

B.J.T., A.E.C., S.K., and E.G. report that they hold patents related to the technology and analysis methods described in this study. The particular DOS imaging instrumentation used in this study was constructed in a university laboratory by using National Institutes of Health grants. These patents are owned by the University of California. B.J.T. and A.E.C. are members of a scientific advisory board for Volighten (Irvine, Calif) and hold stock in this company. They have licensed these patents to Volighten through the University of California, Irvine. They assert that *(a)* this study was completed prior to the formation of the company Volighten, *(b)* they were not involved with Volighten during the acquisition, processing, and analysis of the results presented in this study, and *(c)* this study was completed without any influence by Volighten. Volighten provided no support (financial or other) toward this study.

Implications for Patient Care

- DOS imaging with the SRDS method may be used in conjunction with other radiologic imaging to characterize abnormal regions in the breast.
- The application of DOS imaging with the SRDS method is simple to perform and can be provided at bedside or with portable technology.

Patients

All patients provided written informed consent to participate in the study in strict adherence to a protocol approved by an institutional review board of the University of California, Irvine. The

Published online
10.1148/radiol.09082134

Radiology 2010; 254:277–284

Abbreviations:
DOS = diffuse optical spectroscopy
NIR = near infrared
SRDS = self-referencing differential spectroscopy
STC = specific tumor component

Author contributions:
Guarantors of integrity of entire study, S.K., B.J.T., E.G.; study concepts/study design or data acquisition or data analysis/interpretation, all authors; manuscript drafting or manuscript revision for important intellectual content, all authors; manuscript final version approval, all authors; literature research, S.K., D.H.; clinical studies, W.T., D.H.; experimental studies, D.H., E.G.; statistical analysis, S.K., A.E.C., E.G.; and manuscript editing, S.K., A.E.C., D.H., B.J.T., E.G.

Funding:
This work was supported by a National Cancer Institute Network for Translational Research in Optical Imaging grants (nos. U54-CA105480-01 and U54-CA136400), a UCI Cancer Center grant (no. P30-CA62203), a Laser Microbeam and Medical Program grant (no. P41-RR01192), and a National Institutes of Health Laboratory for Fluorescence Dynamics grant (no. P41-RR03155).

See Materials and Methods for pertinent disclosures.

Figure 1

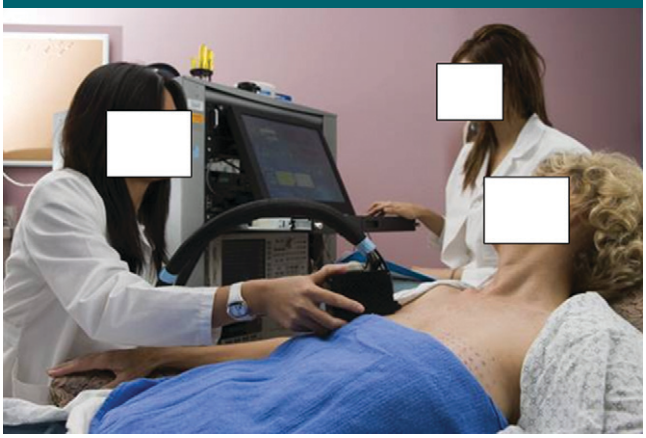

Figure 1: Laser breast scanner has a handheld probe which is placed in gentle contact with the breast during data acquisition. DOS imaging measurements were obtained in both breasts, point by point over a series of lines marked at 10-mm intervals. For the tumor-containing breast, DOS imaging measurements were taken over tumor and surrounding normal tissues. Similar measurements were taken on the mirrored location of the contralateral breast.

Figure 2

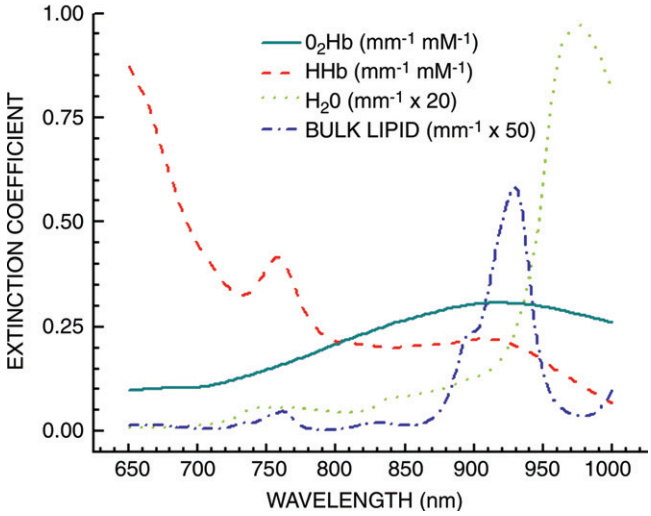

Figure 2: Tissue-absorber basis spectra set used to describe the major tissue components in the breast (hemoglobin, water, and bulk lipids). *HHb* = deoxyhemoglobin, O_2Hb = oxyhemoglobin.

study was compliant with the Health Insurance Portability and Accountability Act. From a search of patient records dating from August 2004 to January 2007, DOS imaging data for 60 subjects were selected; there were 22 malignant tumors, 18 benign tumors (17 patients), and 21 control subjects. Selection criteria from the protocol were as follows: female, older than 21 years, not pregnant, not taking light-sensitive medications, and gave written informed consent. In addition, for patients with lesions, the subject must have had a suspicious finding on a mammogram or sonogram prior to enrollment in the study. All subjects had palpable lesions. Patients were generally referrals from a physician (D.H.).

Tumor disease was confirmed by using standard of care biopsy results, and control subjects had normal mammographic findings. All subjects were women (age range, 22–74 years). Within each group, mean age and range were as follows (Table 1): malignant group (mean age, 39 years; range, 32–65 years), benign group (mean age, 33 years; range, 22–57 years), and normal group (mean age, 42; range, 22–74 years). There was no significant age difference between normal and malignant populations (P = .14). However, the fibroadenoma population age was significantly younger than the normal (P = .04) and malignant (P = .001) age populations. For a subset group of five subjects randomly selected, data were reanalyzed by using a different set of normal tissue as the internal control. We stress that the algorithm takes into account the functional backgrounds of the patients and in principle accounts for age-dependent physiologic effects.

In the control population, 13 were premenopausal, one was perimenopausal, and the remaining seven were postmenopausal.

The selection criteria for DOS imaging were mainly a function of patient convenience. Not all patients in the University of California, Irvine breast clinic were scanned with DOS; patients came to the Beckman Laser Institute and arranged for the DOS imaging independently of their medical treatment. Thus, the 60 subjects were not consecutive patients seen in the University of California, Irvine breast clinic.

DOS imaging measurements were generally obtained prior to or 4 weeks after biopsy to avoid artifacts from bruising. Great care was taken to ensure that the observed DOS imaging signals were not because of biopsy effects. In the malignant population, seven of 22 DOS imaging measurements were obtained prior to biopsy. Of the remaining subjects, the average DOS imaging measurement took place 32 days ± 16 (standard deviation) after biopsy (minimum, 14 days). In the fibroadenoma population, five of 17 patients were measured prior to undergoing biopsy. The average DOS imaging measurement date was 344 days ± 440 after undergoing biopsy (minimum, 40 days).

Instrumentation

The DOS instrument, which uses a combined frequency-domain and continuous-wave tissue spectrometer, has been previously described (29–31). The combined system is necessary to provide absorption and scattering spectra from 650 to 1000 nm (approximately 1000 wavelengths with 8-nm spectral resolution). The frequency-domain light sources are six independent laser diodes (660, 690, 780, 808, 830, and 850 nm), while the continuous-wave light source is a tungsten-halogen lamp. Frequency-modulated light was detected by using an avalanche photodiode detector, and continuous-wave light was detected by using a back-illuminated spectrometer. A handheld probe incorporates source (ie, optical fibers) and detector (ie,

avalanche photodiode detector and a spectrometer detector fiber) channels (Fig 1). Less than 20 mW of optical power was launched into the tissue at any time by using reflection geometry (28-mm source detector separation). Frequency-domain measurements were calibrated with a tissue-simulating phantom with known absorption and scattering properties. Spectral response was calibrated by using a commercial reflectance standard (Spectralon, Labsphere, North Sutton, NH).

Measurement Procedure

DOS imaging measurements were acquired by moving the handheld probe over the tumor in lines of discrete measurement points spaced 10 mm apart (Fig 1). Tumor locations were known a priori from mammographic findings, ultrasonographic (US) findings, and/or palpation. Patients were measured in the supine position. Probe contact was similar to that at US, by using gentle contact on the breast without compression. Full broadband absorption and reduced scattering spectra were measured at each spatial location, requiring less than 10 seconds per spatial location. Similar measurements were taken on the mirrored location of the contralateral breast.

Data Analysis

Data were analyzed by using custom software designed for Matlab (Mathworks, Natick, Mass). For each measured breast location, frequency-domain and continuous-wave data were processed to recover scatter-corrected absorption spectra from 650 to 1000 nm (24). The concentrations of NIR absorbers were calculated from a spectral model of tissue absorption by using the basis spectra (Fig 2). For the self-referencing differential spectroscopy (SRDS) method, the absorption spectra were further analyzed by using custom software (Elantest; Laboratory for Fluorescence Dynamics, Irvine, Calif, *www.lfd.uci.edu*). Details of the SRDS method, also known as the double-differential method, have been described (28). Briefly, the SRDS method depicts spectral components not accounted for by the basis absorber spectra (Fig 2) by eliminating patient-specific spectral variations from scatter-corrected absorption spectra. The unaccounted spectral components are called collectively the specific tumor component (STC) spectrum, because these STC spectra are found only in lesions and not in normal tissues. The STC represents tissue absorption associated with the molecular disposition of NIR absorbers in tissues.

STC spectra were recovered over an average of spatial points for patients with tumors in both lesion and normal areas (see Appendix E1 [online]).

Statistical Analysis

STC spectra for malignant and benign tumors were distinguished by using a custom spectral separation method (see Appendix E1 [online]). In brief, the algorithm maximizes differences in spectral shape by weighting different wavelength regions. For every patient (for each spectrum), the "similarity" from the average STC spectrum of a benign and a malignant lesion was calculated and translated into an index (ie, the malignancy index), which ranged from −1 to 1. Sensitivity, specificity, positive predictive value, and negative predictive value were calculated on the basis of accuracy in benign or malignant classification.

Additional statistical calculations were performed by using commercial software (JMP IN; SAS Institute, Cary, NC). Nonparametric statistics were used to calculate spectral differences between benign and malignant populations (Wilcoxon rank sum test). Significance was assumed at a confidence interval of 95% ($\alpha = .05$) for a two-tailed distribution. All spectral error bars are those for the population.

We analyzed the effect of including an increasing number of spectra in calculating the average. The "score" (ie, the separability of fibroadenoma from cancer) converges to a constant value as the number of patients used for the average was increased. Therefore, we concluded that adding more patients will not further decrease the separability. After a data set of 20, we started to reach a plateau, which is sufficient to separate fibroadenoma from cancer.

The data set was subjected to a round-robin analysis to determine the dependence of the classification of the patients according to the malignancy index on the particular set. Each patient was systematically omitted from the set. For each of the reduced sets (one patient omitted), the weighting factors were optimized. The malignancy index for the omitted patient was calculated according to the new weights as if this patient was unknown. We found that the malignancy index changed slightly for each patient. However, no patient changed classification as a result of this round-robin analysis.

Patient Characteristics of Those Who Underwent DOS Imaging

					Menopausal Status†		
Classification	Age (y)	Body Mass Index (kg/cm^2)	Lesion Size (mm)	US ACR BI-RADS*	Premenopausal	Postmenopausal	Perimenopausal
Cancer	39 (32–65)	28.2 (18.9–40.3)	18 (7–100)	4.81 (4–5)	12	10	NA
Fibroadenoma	33 (22–57)	24.23 (18.64–30.36)	19.9 (4–37)	3.33 (2–4)	14	6	1
Control subject	42 (22–74)	24 (17.8–41.8)	NA	NA	13	7	1

Note.—Unless otherwise indicated, data are means, with ranges in parentheses. NA = not applicable.

* ACR BI-RADS = American College of Radiology Breast Imaging Reporting and Data System.

† Data are numbers of subjects.

Figure 3

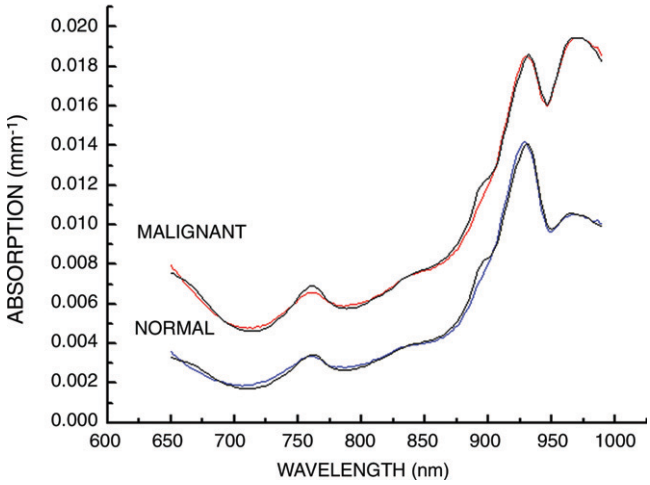

Figure 3: Average of absorption spectra obtained at 11 spatial locations averaged along a line for malignant and normal breast tissues. Experimental absorption data were fit by using a linear combination of the basis spectra (oxyhemoglobin, deoxyhemoglobin, bulk lipid, and water).

Figure 5

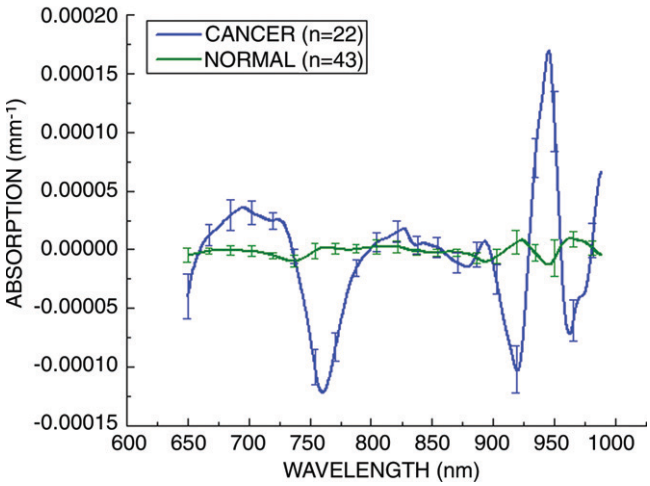

Figure 5: Average STC spectra for 22 malignant tumors and 43 normal tissue regions (21 control subjects, 22 patients with malignant tumors). These spectra have been amplitude normalized. Normal and malignant spectra show discernable and repeatable differences by using the SRDS method. Error bars = distribution of the population.

Figure 4

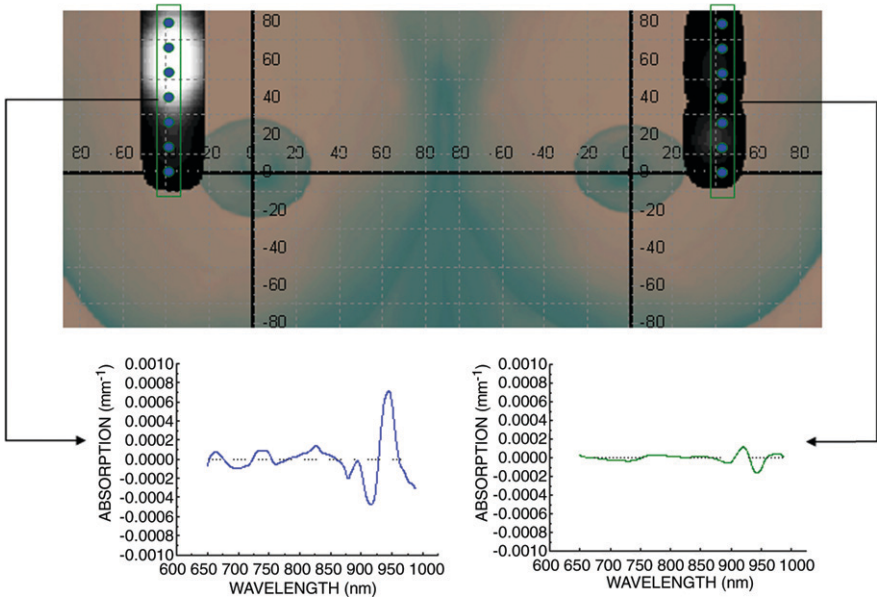

Figure 4: STC index–based image for malignant tumor (11 × 13 mm). DOS imaging–mapped regions of the breast are superimposed onto a breast picture. Vertical boxes indicate a subset of the region of interest corresponding to the spectra below. Dots on the image indicate locations at which DOS imaging measurements were obtained. SRDS spectra are shown in two regions: malignant tissue (left) and normal tissue (right). Note that the STC absorption spectrum is found only in the tumor-containing region and not in the surrounding normal tissue. Thus, the STC spectra were spatially localized.

Results

NIR Tumor Characteristics

In Figure 3, we show an example of NIR absorption spectra averaged over a line of points from tumor-containing and normal tissues. The overall absorption is higher across the spectrum for tumor tissue than that for normal tissue. The increased absorption below 850 nm is attributed to increases in oxy- and deoxyhemoglobin (13–15,24,32). These spectral changes originate from electronic transitions in molecular states. The increased absorption near 960 nm is due to O-H vibrational overtones, which are primarily due to water. Tissue absorption near 930 nm is representative of vibrational overtones of lipid C-H bonds. These spectral features have been documented in a previous study of 58 malignant tumors (24).

Specific Tumor Spectra

SRDS spectra from representative normal (right breast) and malignant (left breast) tissues were calculated at seven spatial locations (Fig 4). The SRDS method uncovered spectral signatures that were not accounted for by the traditional NIR basis set, as demonstrated

Figure 6

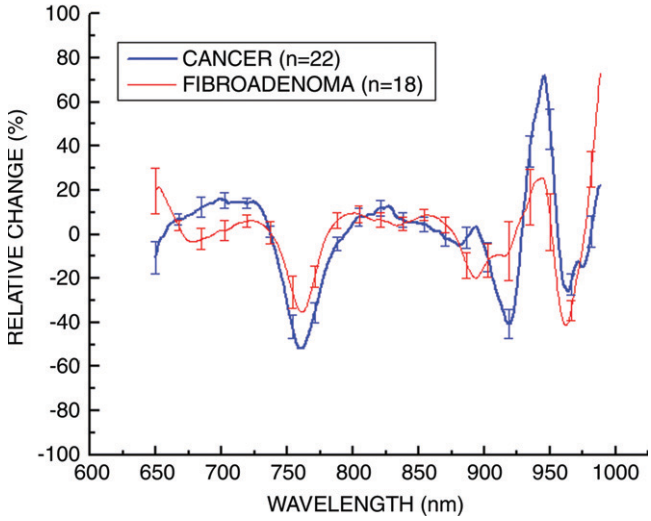

Figure 6: Average STC spectra for 22 malignant tumors and 18 benign lesions. These spectra have been amplitude normalized. Benign and malignant spectra show discernable and repeatable differences by using the SRDS method. Error bars = distribution of the population.

Figure 7

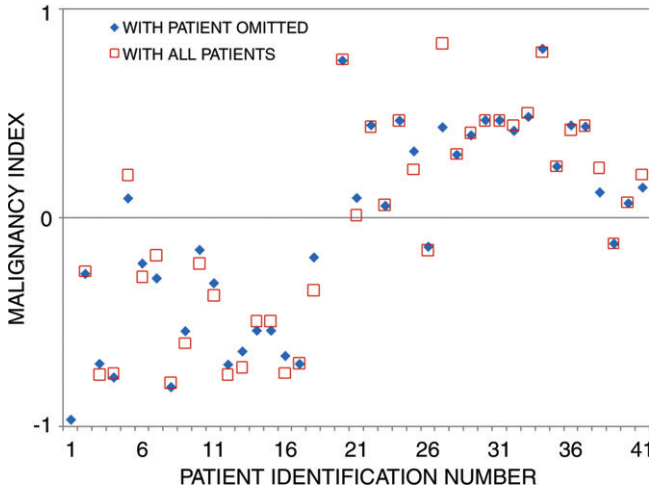

Figure 7: Separation of benign and malignant tumors by using malignancy index. Malignancy index maximizes differences in wavelength regions of STC spectra to separate benign from malignant tumor types. □ = malignancy index for the set using all patients. ◆ = malignancy index for the patients in the round-robin test. Details of the algorithm are given in Appendix E1 (online).

by the spectral features present in the left (malignant) spectrum but absent in the right (normal) spectrum.

Increases in STC index were localized in the region of the tumor and were not present in normal tissue regions. While these maps are relatively low in spatial resolution, they are highly specific for malignancy.

Specific Tumor Spectra and Population Distribution

Figure 5 presents the STC spectra acquired from 22 malignant breast tumors and the spatially equivalent normal tissue from the same patients, as well as normal regions from 21 control subjects. Despite the wide range in patient age and tumor size, the STC spectrum was present in all 22 tumors and was not found in the normal tissues of any subjects in this study. STC spectra were found in all malignant cases and displayed notable features in the following five wavelength regions: 650–665, 730–800, 875–930, 930–960, and 980–1000 nm (28). We note that the specific choice of normal region had little effect on the overall shape of the STC spectrum. The STC spectral shapes were similar to the original, and the tumors were correctly classified as benign or malignant.

In Figure 6, we present a comparison of STC spectra that have been normalized to the amplitude (thereby providing a ratio) to retrieve the differences in spectral shape, as opposed to magnitude, from both benign (n = 18) and malignant (n = 22) tumors. Distinctive spectral differences exist between the STC spectra of these populations.

Differential Diagnosis

The average malignancy index values for benign and malignant tumors were -0.51 ± 0.29 and 0.44 ± 0.26, respectively. These means were statistically different ($Z < .0001$, Wilcoxon rank sum test, two sided, $\alpha = .05$). Plotting the malignancy index values for all patients showed a separation between the pathologic states (Fig 7). The malignancy index was positive for malignant tumors and negative for benign tumors. As shown in Figure 7, one benign tumor (patient 5) was misclassified as cancer and two cancers (patients 25 and 38) were misclassified as benign. If we use a value of 0.0 as the cutoff point, we would recover a sensitivity and specificity of 91% and 94%, respectively. Positive predictive values and negative predictive values were calculated to be 95% and 89%, respectively.

Discussion

Increased spectral content improves tissue characterization. The SRDS approach to spectral analysis revealed spectral signatures that contain specific absorption bands which separate normal from normal tissue and benign from malignant tissue. To accurately measure these fingerprint STC spectra, it is imperative that many individual NIR wavelengths (approximately 1000) are measured across a wide spectral band (650–1000 nm). The amplitudes of the STC spectra are small (about 1% of the total absorption) but well above the signal-to-noise ratio. The STC spectral shapes are highly reproducible and exhibit consistent and specific wavelength-dependent characteristics. In STC spectra, the variations in abundance of NIR absorbers resulting from interpatient variances have been effectively subtracted (28). This self-referencing feature is important because NIR absorption spectra are known to

depend on patient age and hormonal status (24,26,27).

The SRDS method is adaptable in that the normal tissue need not be from the contralateral breast. Normal tissue from the tumor side can be used for the analysis, such as for one patient for whom data were not available from the contralateral side and for one patient who had bilateral tumors. Furthermore, the specific choice of normal tissue is not critical. The SRDS may also help characterize lesions in the areolar complex; some investigators (16) have reported reduced sensitivity due to the increased attenuation from glandular tissue. Given that the SRDS method relies on the differences in tissue regions, the effect of the areola can be corrected.

STC absorption bands obtained by using the SRDS method depict and/or characterize tumors by the presence of a specific endogenous spectral signature. In contrast, NIR absorption spectra have traditionally depicted tumors by thresholding levels of hemoglobin concentration and/or saturation. While increased levels of hemoglobin are often found in malignant breast tissues, hemoglobin is not a specific marker for tumors. Thus, the STC signature arises from changes in molecular disposition, not abundance. No tomography or reconstructions were needed to recover STC spectra.

Shape detection has several advantages over abundance detection. We found that the shape of the STC spectra was conserved, regardless of size of tumor (4–43 mm in the largest dimension). While the depth of the tumor was not available, we hypothesize that the tumor depth affects the amplitude of STC spectra but not the spectral shape. Conservation of STC shape is an important consequence of the SRDS analysis, which subtracts normal physiologic variation. SRDS tumor depiction and/or classification is based solely on the presence of a spectral signature (ie, the background is zero). Furthermore, the shape preservation in the SRDS method implies that detection is limited only by the signal-to-noise ratio of the instrument. In contrast, thresholding used by conventional optical detection depends on the magnitude of the physiologic background.

By using the STC signature alone, we misclassified three of 40 tumors analyzed in this study (two false-negative findings, one false-positive finding). These misclassifications in signal may arise from tumor heterogeneity or other unknown spectral components. Additional information from other optical parameters such as concentrations of hemoglobin, water, and bulk lipid may improve classification. Furthermore, DOS imaging may be combined with other imaging modalities to improve sensitivity and specificity.

On the basis of the wavelength dependence of the STC spectrum, we hypothesize that the signature is due to changes in lipid metabolism. Recent studies (10,33–35) have shown that cancers can alter the lipid metabolism. Benign lesions such as fibroadenomas display hemodynamic signatures similar to those of malignant lesions (16,25).

There were limitations to the study. Fibroadenomas were the only type of benign tumors measured. Furthermore, the lesions were not corrected for depth.

In conclusion, the SRDS method relies on the presence or absence of a spectral fingerprint that reports on molecular disposition and not molecular abundance. These changes in molecular disposition are on the order of parts per thousand and are possibly due to alterations in the lipid state. The SRDS technique subtracts for the unique metabolism of each individual patient and facilitates comparisons across patient populations. We converted the observed molecular dispositions into a simple index that stratified benign and malignant tumors in a population of 40 subjects with lesions. The observation of pathologic state–specific spectral signatures provided a potentially significant method for differential diagnosis and monitoring response to therapy.

Acknowledgments: Programmatic support was provided by the Air Force Office of Scientific Research Medical Free Electron Laser program and the Beckman Foundation. We thank our staff at the Beckman Laser Institute for assisting with acquisition of measurements and subjects for participating in research.

References

1. Gribbestad IS, Sitter B, Lundgren S, Krane J, Axelson D. Metabolite composition in breast tumors examined by proton nuclear magnetic resonance spectroscopy. Anticancer Res 1999;19:1737–1746.
2. Roebuck JR, Cecil KM, Schnall MD, Lenkinski RE. Human breast lesions: characterization with proton MR spectroscopy. Radiology 1998;209:269–275.
3. Kvistad KA, Bakken IJ, Gribbestad IS, et al. Characterization of neoplastic and normal human breast tissues with in vivo (1)H MR spectroscopy. J Magn Reson Imaging 1999;10:159–164.
4. Jagannathan NR, Kumar M, Seenu V, et al. Evaluation of total choline from in-vivo volume localized proton MR spectroscopy and its response to neoadjuvant chemotherapy in locally advanced breast cancer. Br J Cancer 2001;84:1016–1022.
5. Yeung DK, Chan Y, Leung S, Poon PM, Pang C. Detection of an intense resonance at 2.4 ppm in 1H MR spectra of patients with severe late-delayed, radiation-induced brain injuries. Magn Reson Med 2001;45:994–1000.
6. Cecil KM, Schnall MD, Siegelman ES, Lenkinski RE. The evaluation of human breast lesions with magnetic resonance imaging and proton magnetic resonance spectroscopy. Breast Cancer Res Treat 2001;68:45–54.
7. Tse GM, Yeung DK, King AD, Cheung HS, Yang WT. In vivo proton magnetic resonance spectroscopy of breast lesions: an update. Breast Cancer Res Treat 2007;104:249–255.
8. Bolan PJ, Meisamy S, Baker EH, et al. In vivo quantification of choline compounds in the breast with 1H MR spectroscopy. Magn Reson Med 2003;50:1134–1143.
9. Kim JK, Park SH, Lee HM, et al. In vivo 1H-MRS evaluation of malignant and benign breast diseases. Breast 2003;12:179–182.
10. Meisamy S, Bolan PJ, Baker EH, et al. Neoadjuvant chemotherapy of locally advanced breast cancer: predicting response with in vivo (1)H MR spectroscopy—a pilot study at 4 T. Radiology 2004;233:424–431.
11. Kumar M, Jagannathan NR, Seenu V, Dwivedi SN, Julka PK, Rath GK. Monitoring the therapeutic response of locally advanced breast cancer patients: sequential in vivo proton MR spectroscopy study. J Magn Reson Imaging 2006;24:325–332.
12. Manton DJ, Chaturvedi A, Hubbard A, et al. Neoadjuvant chemotherapy in breast

cancer: early response prediction with quantitative MR imaging and spectroscopy. Br J Cancer 2006;94:427–435.

13. Pogue BW, Poplack SP, McBride TO, et al. Quantitative hemoglobin tomography with diffuse near-infrared spectroscopy: pilot results in the breast. Radiology 2001; 218:261–266.

14. Taroni P, Danesini G, Torricelli A, Pifferi A, Spinelli L, Cubeddu R. Clinical trial of time-resolved scanning optical mammography at 4 wavelengths between 683 and 975 nm. J Biomed Opt 2004;9:464–473.

15. Chance B, Nioka S, Zhang J, et al. Breast cancer detection based on incremental biochemical and physiological properties of breast cancers: a six-year, two-site study. Acad Radiol 2005;12:925–933.

16. Zhu Q, Cronin EB, Currier AA, et al. Benign versus malignant breast masses: optical differentiation with US-guided optical imaging reconstruction. Radiology 2005;237:57–66.

17. Grosenick D, Wabnitz H, Moesta KT, Mucke J, Schlag PM, Rinneberg H. Time-domain scanning optical mammography. II. Optical properties and tissue parameters of 87 carcinomas. Phys Med Biol 2005;50:2451–2468.

18. Xu RX, Povoski SP. Diffuse optical imaging and spectroscopy for cancer. Expert Rev Med Devices 2007;4:83–95.

19. Choe R, Corlu A, Lee K, et al. Diffuse optical tomography of breast cancer during neoadjuvant chemotherapy: a case study with comparison to MRI. Med Phys 2005; 32:1128–1139.

20. Zhu Q, Kurtzma SH, Hegde P, et al. Utilizing optical tomography with ultrasound localization to image heterogeneous hemoglobin distribution in large breast cancers. Neoplasia 2005;7:263–270.

21. Cerussi AE, Jakubowski D, Shah N, et al. Spectroscopy enhances the information content of optical mammography. J Biomed Opt 2002;7:60–71.

22. Cerussi A, Hsiang D, Shah N, et al. Predicting response to breast cancer neoadjuvant chemotherapy using diffuse optical spectroscopy. Proc Natl Acad Sci U S A 2007;104:4014–4019.

23. Shah N, Gibbs J, Wolverton D, Cerussi A, Hylton N, Tromberg BJ. Combined diffuse optical spectroscopy and contrast-enhanced magnetic resonance imaging for monitoring breast cancer neoadjuvant chemotherapy: a case study. J Biomed Opt 2005;10:051503.

24. Cerussi A, Shah N, Hsiang D, Durkin A, Butler J, Tromberg BJ. In vivo absorption, scattering, and physiologic properties of 58 malignant breast tumors determined by broadband diffuse optical spectroscopy. J Biomed Opt 2006;11:044005.

25. Intes X. Time-domain optical mammography SoftScan: initial results. Acad Radiol 2005;12:934–947.

26. Pogue BW, Jiang S, Dehghani H, et al. Characterization of hemoglobin, water, and NIR scattering in breast tissue: analysis of intersubject variability and menstrual cycle changes. J Biomed Opt 2004;9:541–552.

27. Cubeddu R, D'Andrea C, Pifferi A, Taroni P, Torricelli A, Valentini G. Effects of the menstrual cycle on the red and near-infrared optical properties of the human breast. Photochem Photobiol 2000;72:383–391.

28. Kukreti S, Cerussi A, Tromberg B, Gratton E. Intrinsic tumor biomarkers revealed by novel double-differential spectroscopic analysis of near-infrared spectra. J Biomed Opt 2007; 12:020509.

29. Pham TH, Coquoz O, Fishkin JB, Anderson E, Tromberg BJ. Broad bandwidth frequency domain instrument for quantitative tissue optical spectroscopy. Rev Sci Instrum 2000; 71:2500–2513.

30. Bevilacqua F, Berger AJ, Cerussi AE, Jakubowski D, Tromberg BJ. Broadband absorption spectroscopy in turbid media by combined frequency-domain and steady-state methods. Appl Opt 2000;39:6498–6507.

31. Jakubowski DB, Cerussi AE, Bevilacqua F, et al. Monitoring neoadjuvant chemotherapy in breast cancer using quantitative diffuse optical spectroscopy: a case study. J Biomed Opt 2004;9:230–238.

32. Franceschini MA, Moesta KT, Fantini S, et al. Frequency-domain techniques enhance optical mammography: initial clinical results. Proc Natl Acad Sci U S A 1997;94:6468–6473.

33. Katz-Brull R, Lavin PT, Lenkinski RE. Clinical utility of proton magnetic resonance spectroscopy in characterizing breast lesions. J Natl Cancer Inst 2002;94:1197–1203.

34. Kleinfeld AM, Okada C. Free fatty acid release from human breast cancer tissue inhibits cytotoxic T-lymphocyte-mediated killing. J Lipid Res 2005;46:1983–1990.

35. Chow LW, Cheng CW, Wong JL, Toi M. Serum lipid profiles in patients receiving endocrine treatment for breast cancer: the results from the Celecoxib Anti-Aromatase Neoadjuvant (CAAN) Trial. Biomed Pharmacother 2005;59(suppl 2): S302–S305.